Research Article | Vol. 25, No. 4 | 20 Feb 2017 | OPTICS EXPRESS 4403
Optics EXPRESS

Fourier transform spectroscopy in the vibrational fingerprint region with a birefringent interferometer

J. RÉHAULT,[1,5] R. BORREGO-VARILLAS,[2] A. ORIANA,[3] C. MANZONI,[2] C. P. HAURI,[1] J. HELBING,[4] AND G. CERULLO[2,6]

[1]*Paul Scherrer Institute, SwissFEL, 5232 Villigen, Switzerland*
[2]*IFN-CNR, Politecnico di Milano, Piazza Leonardo da Vinci, Milano, Italy*
[3]*Laboratoire de Spectroscopie Ultrarapide, EPFL, CH-1015 Lausanne, Switzerland*
[4]*University of Zurich, Department of Chemistry, Winterthurerstrasse 190, CH-8057 Zurich, Switzerland*
[5]*julien.rehault@psi.ch*
[6]*giulio.cerullo@polimi.it*

Abstract: We introduce a birefringent interferometer for Fourier transform (FT) spectroscopy in the mid-infrared, covering the vibrational fingerprint region (5-10 μm, 1000-2000 cm^{-1}), which is crucial for molecular identification. Our interferometer employs the crystal calomel (Hg_2Cl_2), which combines high birefringence (n_e-n_o≈0.55) with a broad transparency range (0.38-20 μm). We adopt a design based on birefringent wedges, which is simple and compact and guarantees excellent delay accuracy and long-term stability. We demonstrate FTIR spectroscopy, with a frequency resolution of 3 cm^{-1}, as well as two-dimensional IR (2DIR) spectroscopy. Our setup can be extended to other spectroscopic modalities such as vibrational circular dichroism and step-scan FT spectroscopy.

OCIS codes: (300.6300) Spectroscopy, Fourier transforms; (300.6340) Spectroscopy, infrared; (300.6530) Spectroscopy, ultrafast; (260.1440) Birefringence; (120.3180) Interferometry.

References and links

1. S. P. Davis, M. C. Abrams, and J. W. Brault, *Fourier Transform Spectrometry* (Academic Press, 2001).
2. P. B. Fellgett, "On the ultimate sensitivity and practical performance of radiation detectors," J. Opt. Soc. Am. **39**(11), 970–976 (1949).
3. P. Jacquinot, "New developments in interference spectroscopy," Rep. Prog. Phys. **23**(1), 267–312 (1960).
4. P. Connes, "Astronomical Fourier spectroscopy," Annu. Rev. Astron. Astrophys. **8**(1), 209–230 (1970).
5. B. C. Smith, *Fundamentals of Fourier Transform Infrared Spectroscopy* (CRC Press, 2011).
6. L. A. Nafie, *Vibrational Optical Activity* (John Wiley & Sons, 2011).
7. K. Ataka, T. Kottke, and J. Heberle, "Thinner, smaller, faster: IR techniques to probe the functionality of biological and biomimetic systems," Angew. Chem. Int. Ed. Engl. **49**(32), 5416–5424 (2010).
8. P. Hamm and M. T. Zanni, *Concepts and Methods of 2D Infrared Spectroscopy* (Cambridge University, 2011).
9. R. J. Bell, *Introductory Fourier Transform Spectroscopy* (Elsevier, 2012).
10. L. Mertz, "Astronomical photoelectric spectrometer," Astron. J. **71**, 749–751 (1966).
11. M. F. A'Hearn, F. J. Ahern, and D. M. Zipoy, "Polarization fourier spectrometer for astronomy," Appl. Opt. **13**(5), 1147–1157 (1974).
12. M. J. Padgett and A. R. Harvey, "A static Fourier-transform spectrometer based on Wollaston prisms," Rev. Sci. Instrum. **66**(4), 2807–2811 (1995).
13. X. Lin, F. Zhou, H. Li, and H. Zhao, "Static Fourier-transform spectrometer based on Wollaston prism," Int. J. Light Electron Opt. **125**(14), 3482–3484 (2014).
14. A. Harvey and D. Fletcher-Holmes, "Birefringent Fourier-transform imaging spectrometer," Opt. Express **12**(22), 5368–5374 (2004).
15. M. W. Kudenov and E. L. Dereniak, "Compact real-time birefringent imaging spectrometer," Opt. Express **20**(16), 17973–17986 (2012).
16. A. Oriana, J. Réhault, F. Preda, D. Polli, and G. Cerullo, "Scanning Fourier transform spectrometer in the visible range based on birefringent wedges," J. Opt. Soc. Am. A **33**(7), 1415–1420 (2016).
17. D. Brida, C. Manzoni, and G. Cerullo, "Phase-locked pulses for two-dimensional spectroscopy by a birefringent delay line," Opt. Lett. **37**(15), 3027–3029 (2012).
18. J. Réhault, M. Maiuri, A. Oriana, and G. Cerullo, "Two-dimensional electronic spectroscopy with birefringent wedges," Rev. Sci. Instrum. **85**(12), 123107 (2014).

#283351 https://doi.org/10.1364/OE.25.004403
Journal © 2017 Received 20 Dec 2016; revised 6 Feb 2017; accepted 7 Feb 2017; published 16 Feb 2017

Optics EXPRESS

19. R. Borrego-Varillas, A. Oriana, L. Ganzer, A. Trifonov, I. Buchvarov, C. Manzoni, and G. Cerullo, "Two-dimensional electronic spectroscopy in the ultraviolet by a birefringent delay line," Opt. Express **24**(25), 28491–28499 (2016).
20. J. Réhault, M. Maiuri, C. Manzoni, D. Brida, J. Helbing, and G. Cerullo, "2D IR spectroscopy with phase-locked pulse pairs from a birefringent delay line," Opt. Express **22**(8), 9063–9072 (2014).
21. F. Preda, V. Kumar, F. Crisafi, D. G. Figueroa Del Valle, G. Cerullo, and D. Polli, "Broadband pump-probe spectroscopy at 20-MHz modulation frequency," Opt. Lett. **41**(13), 2970–2973 (2016).
22. J. Réhault, F. Crisafi, V. Kumar, G. Ciardi, M. Marangoni, G. Cerullo, and D. Polli, "Broadband stimulated Raman scattering with Fourier-transform detection," Opt. Express **23**(19), 25235–25246 (2015).
23. C. Barta, "Preparation of Mercurous Chloride Monocrystals," Krist. Tech. **5**(4), 541–549 (1970).
24. M. Gottlieb, A. P. Goutzoulis, and N. B. Singh, "Fabrication and characterization of mercurous chloride acoustooptic devices," Appl. Opt. **26**(21), 4681–4687 (1987).
25. R. Maksimenka, P. Nuernberger, K. F. Lee, A. Bonvalet, J. Milkiewicz, C. Barta, M. Klima, T. Oksenhendler, P. Tournois, D. Kaplan, and M. Joffre, "Direct mid-infrared femtosecond pulse shaping with a calomel acousto-optic programmable dispersive filter," Opt. Lett. **35**(21), 3565–3567 (2010).
26. L. P. DeFlores, R. A. Nicodemus, and A. Tokmakoff, "Two-dimensional Fourier transform spectroscopy in the pump-probe geometry," Opt. Lett. **32**(20), 2966–2968 (2007).
27. S.-H. Shim, D. B. Strasfeld, Y. L. Ling, and M. T. Zanni, "Automated 2D IR spectroscopy using a mid-IR pulse shaper and application of this technology to the human islet amyloid polypeptide," Proc. Natl. Acad. Sci. U.S.A. **104**(36), 14197–14202 (2007).
28. J. Helbing and P. Hamm, "Compact implementation of Fourier transform two-dimensional IR spectroscopy without phase ambiguity," J. Opt. Soc. Am. B **28**(1), 171–178 (2011).
29. Z. B. Perekalina, C. Barta, I. Gretora, A. B. Wasiljew, and I. D. Kislowskij, "Dichroism and birefringence of Calomel through all regions of its transmittance," Opt. Spectrosc. **42**, 653–655 (1977).
30. T. Brixner, T. Mančal, I. V. Stiopkin, and G. R. Fleming, "Phase-stabilized two-dimensional electronic spectroscopy," J. Chem. Phys. **121**(9), 4221–4236 (2004).
31. A. M. Woys, S. S. Mukherjee, D. R. Skoff, S. D. Moran, and M. T. Zanni, "A strongly absorbing class of non-natural labels for probing protein electrostatics and solvation with FTIR and 2D IR spectroscopies," J. Phys. Chem. B **117**(17), 5009–5018 (2013).
32. I. Peran, T. Oudenhoven, A. M. Woys, M. D. Watson, T. O. Zhang, I. Carrico, M. T. Zanni, and D. P. Raleigh, "General strategy for the bioorthogonal incorporation of strongly absorbing, solvation-sensitive infrared probes into proteins," J. Phys. Chem. B **118**(28), 7946–7953 (2014).
33. C. Rödig and F. Siebert, "Errors and Artifacts in Time-Resolved Step-Scan FT-IR Spectroscopy," Appl. Spectrosc. **53**(8), 893–901 (1999).
34. P. L. Polavarapu, Z. Deng, and G.-C. Chen, "Polarization-Division Interferometry: Time-Resolved Infrared Vibrational Dichroism Spectroscopy," Appl. Spectrosc. **49**(2), 229–236 (1995).
35. H. Rhee, Y.-G. June, J.-S. Lee, K.-K. Lee, J.-H. Ha, Z. H. Kim, S.-J. Jeon, and M. Cho, "Femtosecond characterization of vibrational optical activity of chiral molecules," Nature **458**(7236), 310–313 (2009).
36. B. Dutta and J. Helbing, "Optimized interferometric setup for chiral and achiral ultrafast IR spectroscopy," Opt. Express **23**(12), 16449–16465 (2015).

1. Introduction

Fourier transform (FT) spectroscopy [1] is a powerful technique to measure spectra in the time domain, by recording the interferogram of two delayed replicas of an optical waveform and performing the FT of the delay-dependent signal. With respect to frequency-domain spectrometers, which combine diffraction gratings with single or multi-channel detectors, FT spectrometers have a number of advantages: (i) higher signal to noise ratio for the detection regimes in which sensitivity is limited by detector noise (the Felgett advantage [2]); (ii) higher optical throughput, due to the lack of entrance and exit slits in the monochromator (the Jacquinot advantage [3]); (iii) better frequency accuracy after calibration (the Connes advantage [4]); (iv) the possibility of easily adjusting the frequency resolution by varying the scan range of the interferogram.

FT spectroscopy is particularly advantageous in the mid-infrared (mid-IR) spectral region, from 3 to 10 μm, which allows for accurate fingerprinting of molecules from their characteristic vibrational absorption spectra [5]. The Felgett advantage is fully exploited, because detectors for the mid-IR range are noisy, and array detectors are very expensive. FTIR spectroscopy is a powerful analytical technique, which is widely used in chemistry labs, as well as in a number of applications such as environmental and geological sensing, in some cases also with portable devices. In addition to absorption, the FT approach can be applied to a number of more sophisticated IR spectroscopies: vibrational circular dichroism (VCD) [6],

Optics EXPRESS

which detects the difference between vibrational absorption spectra of left and right circularly polarized light and is a probe of molecular structure and chirality; step-scan FTIR spectroscopy [7], which records transient IR absorption spectra and is a powerful tool to study structural dynamics on the nanosecond to microsecond timescale during photo-induced reactions; two-dimensional infrared (2DIR) spectroscopy. Coherent 2DIR spectroscopy is best understood as a pump-probe technique, which measures the absorption changes after vibrational excitation of a sample as a function of both probe and excitation frequency [8]. This yields 2D-correlation maps, which provide information on molecular structure and dynamics: for example, a sample excited at the frequency of normal mode *a* may instantaneously also show an absorption change at the frequency of mode *b,* as an indication of the (orientation and distance-dependent) coupling of the two modes. The probe frequency in 2DIR is usually measured by dispersing an ultrashort probe pulse after it has crossed the sample. The excitation frequency can be obtained by FT when the probe intensity is recorded as a function of the delay between two replicas of a spectrally broad excitation pulse.

Typically, FTIR spectrometers generate the replicas by a Michelson interferometer (MI) [9], which splits the input beam into two paths that are reflected back by mirrors and recombined at the beam splitter after introducing a time delay. In order to record an accurate interferogram, the difference of the two paths must be controlled or monitored to within a small fraction of the optical wavelength λ (typically λ/50 or better). This requires building a very stable mechanical setup and measuring the delay with an auxiliary visible laser beam, to keep track of the unavoidable path-length fluctuations. This increases the complexity, size and cost of the instrument and potentially limits its portability.

These difficulties can be overcome by the use of birefringent interferometers, which achieve, in a passive way, high long-term stability between the generated replicas. These interferometers, instead of separating the two beam replicas in space, as in the MI, project them onto two perpendicular polarizations, which are delayed by varying the thickness of a birefringent material. The replicas are then projected back to a common polarization state, to allow their interference on the detector. Birefringent interferometers, originally developed for astronomical applications [10, 11], have been used in a variety of configurations, both dynamical and static [12, 13], as well as in imaging modality [14, 15].

We recently demonstrated a passive birefringent interferometer for FT spectroscopy [16], based on a simplified version of the Translating-Wedge-based Identical pulses eNcoding System (TWINS), developed by some of the authors for 2D electronic spectroscopy (2DES) [17]. TWINS has the advantages of being inherently stable, compact and potentially low cost, and we have proved its applicability to a number of spectroscopic methods, including 2DES in the visible [18] and the UV [19], 2DIR spectroscopy [20], FT spectroscopy [16], broadband pump-probe spectroscopy [21] and stimulated Raman scattering spectroscopy [22]. So far two birefringent materials have been used for TWINS, alpha barium borate (α-BBO) and lithium niobate ($LiNbO_3$). Due to their limited transparency range, these materials only work for wavelengths shorter than ~5 μm, thus precluding the mid-IR fingerprint region (5-10 μm, corresponding to 1000-2000 cm^{-1}), which is crucial for molecular identification and FTIR spectroscopy. Extending the TWINS design, and more generally birefringent interferometers, to these wavelengths requires identification of a birefringent material with extended IR transparency.

In this paper we present a TWINS interferometer based on the birefringent crystal mercurous chloride (Hg_2Cl_2), also known as calomel [23–25], which combines a very large birefringence ($\Delta n \approx 0.55$) with a broad transparency range (from 400 nm to 20 μm). We demonstrate the application of the calomel TWINS to both FTIR spectroscopy, achieving a frequency resolution of 3 cm^{-1}, and 2DIR spectroscopy, with full tunability across the vibrational fingerprint region. We find that the calomel TWINS preserves in the mid-IR the advantages (compactness, long-term stability, delay reproducibility) of its versions in the visible.

Optics EXPRESS

2. Experimental setup

The principle of TWINS has been explained in detail in previous articles [16–18]. Briefly, as illustrated in Fig. 1(a), it consists of two blocks, A and B, of the same birefringent material, with optical axes rotated by 90° with respect to each other and perpendicular to the propagation direction of the beam. For an input beam polarized at 45° with respect to the optical axes, block A introduces a fixed delay between the two orthogonally polarized components that propagate along the fast and slow axis of the material. Block B introduces a delay of opposite sign with respect to block A, allowing one to achieve zero delay. To enable fine tuning of the delay, block B is shaped in the form of two wedges with the same apex angle. It should be noted that the displacement of the wedge in block B induces a small lateral displacement and separation of ordinary and extraordinary beams. This leads to a slight loss of fringe contrast at large delays, which, however, did not significantly reduce our frequency resolution. Furthermore, despite the prism-like shape of the wedges, the spatial chromatic dispersion of the beam is negligible given the flat dispersion of Calomel in the mid-IR range.

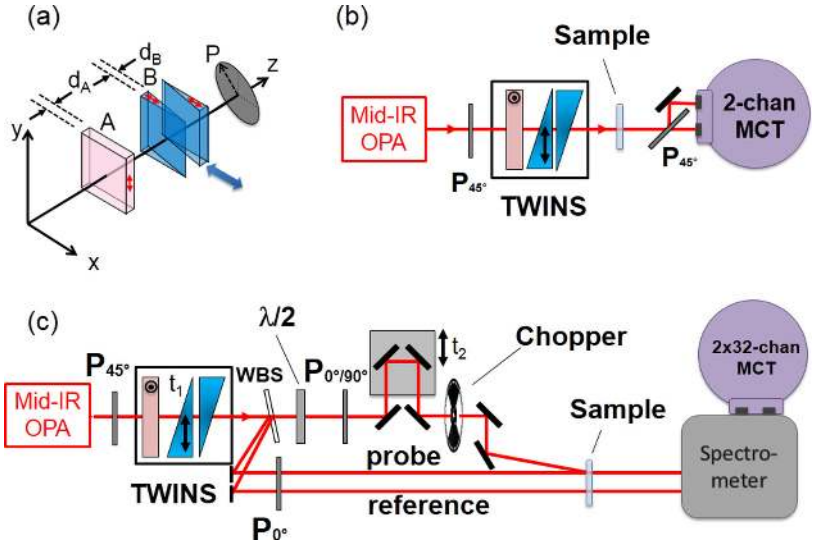

Fig. 1. (a) TWINS interferometer, red arrows and dot represent the optical axes; $P_{45°}$ polarizer at 45° with respect to the horizontal direction; (b) Scheme of the FTIR setup using TWINS; (c) 2DIR setup. $P_{0°}$and $P_{90°}$, polarizer at 0° and 90° with respect to the horizontal, respectively; WBS, wedged beam splitter.

Finally, a polarizer projects the two orthogonal polarizations to a common polarization state, allowing their interference on the detector. Neglecting Fresnel losses of the components, TWINS has the same optical throughput of a MI. When translating one of the wedges in block B by ΔL, the delay variation of the two replicas is [17, 18]:

$$\Delta\tau_{TWINS} = \left(\frac{1}{v_{ge}} - \frac{1}{v_{go}}\right)\Delta L \tan\alpha = \frac{(n_{ge} - n_{go})\Delta L \tan\alpha}{c}$$

where α is the apex angle of the wedges, c is the speed of light in vacuum and v_{go} (v_{ge}) and n_{go} (n_{ge}) are the group velocity and the group refractive index of the ordinary (extraordinary) polarization, respectively. As a comparison, a standard MI introduces, for a translation by ΔL of one of the mirrors, a delay $\Delta\tau_{MI} = \frac{2\Delta L}{c}$. In TWINS the delay is thus demultiplied, with respect to a classical MI, by the so-called gear ratio:

Optics EXPRESS

$$G = \frac{2}{(n_{ge} - n_{go})\tan\alpha}$$

A large value of G guarantees a very high delay accuracy of the interferometer even with standard translation stages and without using position tracking schemes; on the other hand it limits the maximum achievable delay for a given transverse size of the wedges. For our previous TWINS designs in the visible, we had $G \approx 30$-60, resulting in positioning accuracy of the order of λ/300. Here we had to take into account the difficulty in processing calomel in large sizes [23, 24] and the need to achieve large Δτ for high frequency resolution in FTIR. The calomel TWINS were manufactured by BBT-Materials Processing Ltd. with an apex angle $\alpha = 16°$ which, considering a birefringence $\Delta n_g = n_{ge} - n_{go} \approx 0.55$ in the mid-IR range, results in a gear ratio $G \approx 12$. This is still sufficient for our applications, as it translates into a delay accuracy of λ/600 (at 5 μm) for a standard translation stage with 100-nm unidirectional positioning accuracy. With a 20-mm transverse size of the wedges and a 5 mm beam size, the maximum achievable delay in the mid-IR is $\Delta\tau_{max} \approx 7.5$ ps, which corresponds to a maximum frequency resolution of 2 cm^{-1}, if a single-sided interferogram is recorded.

To test the calomel TWINS we used tunable mid-IR pulses from an optical parametric amplifier (OPA) pumped by an amplified Ti:sapphire laser generating 100-fs pulses at 800 nm and 1-kHz repetition rate. By difference frequency generation between signal and idler of the OPA we obtain pulses tunable between 1000 cm^{-1} (10 μm) and 3800 cm^{-1} (2.6 μm) with 100-fs duration, 200-cm^{-1} FWHM bandwidth and 2-μJ energy. Figure 1(b) shows the scheme of the FTIR spectrometer. Before TWINS, we placed a waveplate and a first polarizer oriented at 45° relative to the optical axes of the birefringent wedges; after the interferometer, a second polarizer at 45° separates spatially two perpendicular polarizations, which are reflected and transmitted, respectively. We monitor these two outputs on the two channels of a liquid-nitrogen cooled Mercury Cadmium Telluride (MCT) detector or two identical pyroelectric detectors. Due to energy conservation, the two interferograms have the same amplitude and are 180° out of phase, which allows us to subtract them in order to double the measured signal and effectively suppress source fluctuations. Indeed, apart from very short delays, where interference is maximal, any fluctuation in light intensity is seen as an increase (decrease) of signal on both detectors, which is suppressed by the subtraction. One of the wedges is mounted on a motorized translation stage (Physik Instrumente model M111.1DG) with 100-nm unidirectional positioning accuracy. In order to monitor the stability of the set-up with high precision, we co-propagated a HeNe laser in parallel with the IR beam, and recorded two photodiode signals in quadrature analogous to our previously employed scheme [20].

Figure 1(c) shows the setup used for 2DIR spectroscopy in the mid-IR, adopting the partially collinear pump-probe geometry [26–28]. Here two collinear pump pulses, delayed by the coherence time t_1, are non-collinearly overlapped with the probe pulse, delayed by the waiting time t_2. The original TWINS design, conceived for 2DES [17, 18], included two additional isotropic wedges one of which is moved in the opposite direction with respect to the wedge of block B. In 2DES these additional wedges served a dual purpose: (i) to maintain constant, to the first order, the group delay dispersion (GDD) introduced by TWINS, thus allowing to compensate for it; (ii) to maintain constant, in an absolute temporal frame, the arrival time of one of the two replicas, so as to allow scanning the coherence time t_1 while keeping fixed the waiting time t_2. For the calomel TWINS, due to manufacturing difficulties, we chose to minimize the number of wedges to only two. We could neglect pulse broadening introduced by propagation in the TWINS thanks to the very low dispersion introduced by calomel in the mid-IR, with GDD = 131(53) fs^2 for 1 mm extraordinary (ordinary) propagation of a 5-μm pulse [29]. As a result, when propagating through 5 mm of calomel, a 100-fs pulse at 5 μm is stretched to a negligible 101.6 (100.3) fs for the extraordinary (ordinary) polarization. In order to maintain constant the waiting time t_2 during a t_1 scan, we

Optics EXPRESS

split off the probe (and reference) pulse only after the wedge the TWINS. With the help of a BaF_2 wedge at Brewster angle and a polarizer, we select the polarization parallel to the slow axis of block B i.e. only light from the second pump pulse is reflected. Thus t_2 is kept constant during the t_1 scan. On the pump side, we inserted a half-wave plate at 22.5° between the wedges and the polarizer. The wave plate rotates the two replica to ± 45° and the polarizer is set to 0° or 90° to produces a pair of pump pulses with polarization either parallel or perpendicular to the probe beam. A chopper is placed in the pump beam to reduce the artefact due to the imperfect polarization state after the wedges (see explanation below in the results section). After the sample, probe and reference pulses are dispersed by a monochromator and detected by a double-array MCT detector with 32 pixels.

We point out that in 2D-spectroscopy pairs of non-birefringent wedges are frequently used for changing the delay between pulse replicas, acting as very precise and reproducible delay stages [30]: however in these cases the replicas are generated by means of gratings or beam splitters, and travel along separate optical paths. This is substantially different from our approach: in the TWINS setup presented here, the birefringent wedge pair itself plays the twofold role of generating and delaying the pulse pair, which travel a common optical path and hence intrinsically have phase-stable delay.

3. Results

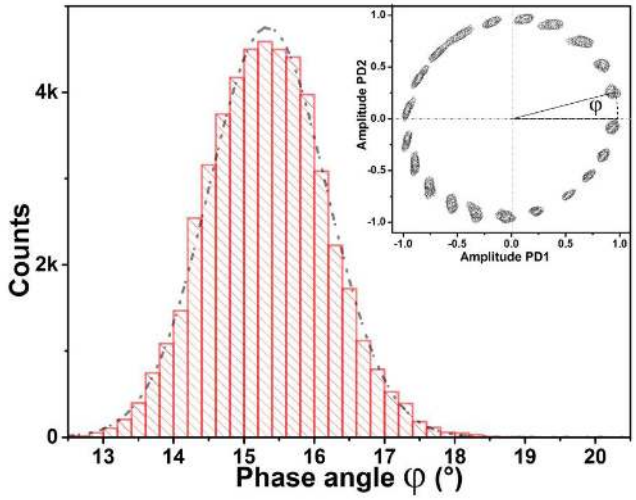

Fig. 2. Statistics on the phase shift introduced by the calomel TWINS on a 632.8-nm He-Ne laser measured on 50000 shots. The distribution has a standard deviation of 0.8°. Inset: stability for 21 positions in a single cycle of a He-Ne fringe, measured on two photodiodes in quadrature (PD signals were normalized after subtraction of the mean signal over many cycles). Each cloud corresponds to 50000 measured laser shots. The circle highlights the position taken for the statistics in the main panel.

We first characterized the phase stability of the calomel TWINS interferometer with a He-Ne laser, using a tracking scheme with two photodiodes, which measure the transmitted intensity of the in quadrature signals [20, 28]. We translated the wedge by fixed increments, and for each step we recorded 50000 consecutive laser shots. The inset of Fig. 2 shows the quadrature plot of the photodiode signals for the 21 steps necessary to scan one cycle of the He-Ne laser, while the main panel of Fig. 2 shows the statistics of the corresponding phase angle for one motor position. The phase standard deviation is ± 0.8°, which corresponds to ± λ/450 fluctuations at 632.8 nm and can be translated to a phase stability of ± λ/2000 at 3μm and ± λ/4000 around 6μm. Next we tested the capability of TWINS to measure mid-IR spectra. Figure 3 shows a series of spectra of the mid-IR pulses generated by the OPA and obtained as the FT of the interferograms. The spectra are tunable from 3 to 10 μm, and show

Optics EXPRESS

characteristic dips arising from the water bending modes near 1600 cm^{-1}, the CO_2 absorption at 2350cm^{-1} and the water stretching lines near 3600 cm^{-1}.

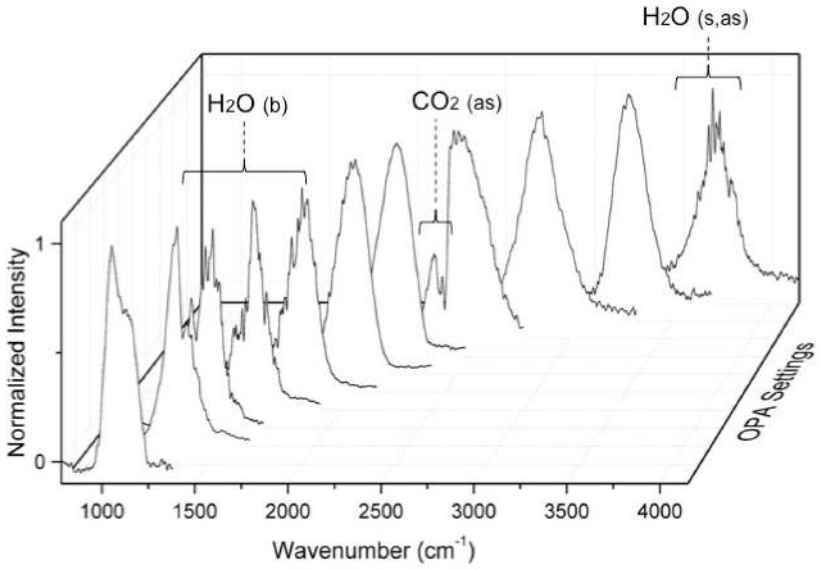

Fig. 3. Sequence of mid-IR spectra obtained tuning the OPA and measured with the TWINS spectrometer, calculated as the average between two forward and two backward scans. We observe clearly the absorption of gaseous H2O and CO2 (s: stretch, as: asymmetric stretch, b: bend). These illustrate the high transmission of Calomel over the mid-IR.

To characterize the frequency resolution of our FTIR setup and its capability to work as an absorption spectrometer, we measured the absorption spectrum of water vapor. To this purpose, we controlled the humidity in our experimental chamber by purging with nitrogen, measured the interferogram and calculated by FT the transmitted mid-IR spectra; measurements were taken at 10% and 30% humidity. The TWINS interferometer was scanned to a maximum delay of 6 ps, corresponding to a spectral resolution of 2.7 cm^{-1}. The resulting absorption spectrum of atmospheric water, obtained as the logarithm of the ratio of the two spectra, is presented in Fig. 4(b) as a black line. To assess the performance of our TWINS spectrometer, we started from a high-resolution absorption spectrum measured with a commercial FTIR spectrometer and applied a low-pass Fourier filter that exactly matches the scan range of our TWINS experiment. The resulting spectrum (Fig. 4(b), red line) shows very good agreement with our measurement.

Optics EXPRESS

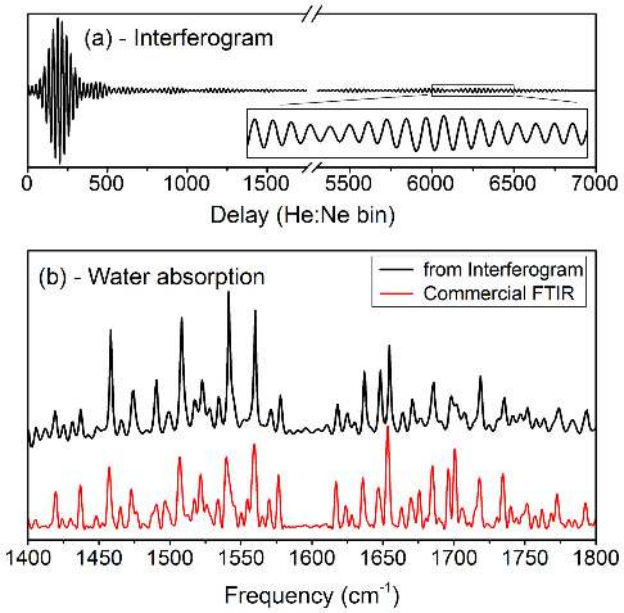

Fig. 4. (a) TWINS interferogram (difference of transmitted and reflected beams from the polarizer) of a 6-μm pulse measured at 30% humidity, averaged over six forward and backward scans and filtered. Horizontal scale corresponds to He-Ne bins, or approximately 1 fs per unit. (b) Absorption spectra of water: comparison between a reference spectrum from a commercial FTIR with resolution of 2.7 cm^{-1} (red line), and a spectrum obtained from two TWINS interferograms recorded at 30% and 10% humidity (black line).

Finally we tested the 2DIR setup based on TWINS. Figure 5 shows the 2DIR spectra of a 50-micrometer-thick sample of a Rhenium carbonyl complex in dimethyl sulfoxide, which was recently introduced as an IR-label for proteins [31, 32].Two identical pump-pulses were created by the birefringent wedges and the delay t_1 between them (the coherence time) was scanned continuously from −0.3 to 3 ps. The 2D spectrum is given by the FT of the probe beam intensity along t_1, and the frequency axis defined by this FT is the horizontal axis in Fig. 5. It indicates at which frequency the sample was excited. The resolution in the horizontal excitation axis is 5 cm^{-1}, which matches the spectrometer resolution along the vertical probe axis. We monitored and calibrated the t_1 delay analogously to our previous study [20] with the help of the co-propagating He-Ne laser and quadrature counting. The three carbonyl groups displayed in Fig. 5(g) give rise to three normal modes: the symmetric stretch at 2019 cm^{-1}, and two asymmetric stretch modes near 1921 cm^{-1}. The latter are nearly degenerate (because of the quasi C_{3v} symmetry of the chromophore) but are nevertheless nicely resolved on the diagonal of the 2DIR spectra. The diagonal peaks arise from molecules which have remained in the same excited state after excitation by the pump-pulse pair to the $v = 1$ level of one of the three normal modes. They consist of a (negative, blue) contribution due to bleach and stimulated emission of the 0-1 transition and a positive (red) contribution due to excited state absorption (1-2 transition), which is lower in frequency due to the anharmonicity of the oscillators. The three normal modes are strongly coupled, which means that excitation of one causes a significant frequency (down-) shift of the other. This gives rise to the off-diagonal peaks, the top left and bottom right peaks in all spectra. All three transition dipole moments are mutually orthogonal, and the off-diagonal peaks that require excitation of one mode and probing of another, are therefore best visible in the spectra recorded with perpendicular polarizations of pump and probe pulses. At longer waiting times t_2 between excitation and the probe pulse, vibrational energy transfer between the three modes enhances the relative strength of the cross peaks. This process is sensitive to the environment and

Optics EXPRESS

increasing contribution of the cross peaks strongly reduces the initial diagonal tilt of the lower left diagonal signal."

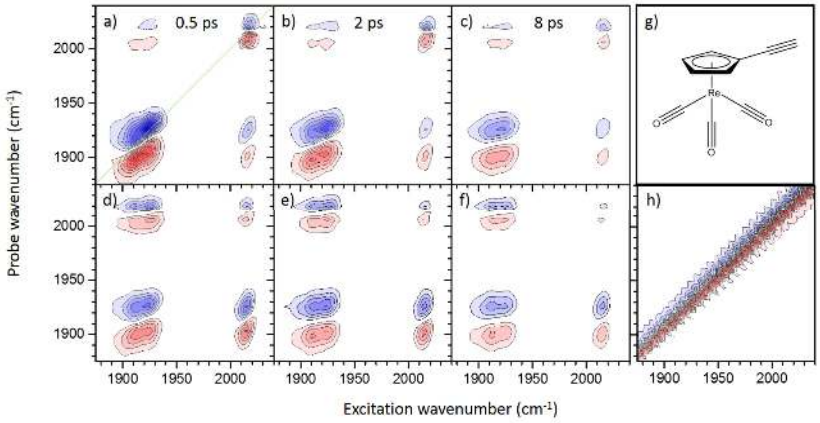

Fig. 5. 2D-IR spectra of the Rhenium carbonyl complex (η^5-HC≡CC$_5$H$_4$)Re(CO)$_3$, see panel g for the chemical formula) at different waiting times. (a-c) parallel polarization, (d-f) perpendicular polarization of pump and probe beams. Contour lines in 10% steps of the largest peak in (a). Negative absorption changes in blue, positive changes in red. (h) Signal due to residual probe interference that is subtracted by chopping. It is 10 times larger than the signal in (a-f) and the color scale has been multiplied by 10 accordingly.

The data demonstrates that high-quality 2DIR spectra can be recorded with a very compact interferometer that consists only of two birefringent wedges and a compensation plate, while the probe pulse is split off only after the pump-pulse pair has been generated. Because of the orthogonal polarizations of the pump pulses, a wedge at Brewster angle selectively reflects only the second of them and residual light from the first pulse is further suppressed by a polarizer. This suppression is, however, not perfect, and the probe (and reference) beam thus contains a very small pre-pulse at a variable time t_1 before the proper probe pulse. During our 2D scans the additional pulse caused a probe intensity modulation of less than 1% (meaning that the pre-pulse would not be visible as an additional probe pulse). Nevertheless, after FT of the t_1 delay, its interference with the probe light gives rise to a large background 2D signal on the diagonal, as shown in Fig. 5(h). This background is, however, very reproducible and can be easily eliminated by chopping the pump beam at half the repetition rate of the laser and subtracting signals with and without excitation. It is even useful as it can be employed to check the calibration of the excitation-frequency axis.

4. Discussion and conclusion

In this paper we have introduced a birefringent interferometer for FT spectroscopy based on the crystal calomel (Hg_2Cl_2) and the TWINS design. The interferometer fully covers the vibrational fingerprint region (5-10 µm, 1000-2000 cm^{-1}) which is crucial for molecular identification. Even longer wavelengths can be covered with an appropriate light source. We demonstrate FTIR spectroscopy with a frequency resolution of ≈3 cm^{-1}, which can be further improved by passing the TWINS wedges twice, or by changing their design. We also demonstrate high signal-to-noise 2DIR spectroscopy with a simplified TWINS setup.

FTIR spectroscopy has experienced many technological improvements since its first commercial implementation in the 1950s and is now a rather mature technology. Commercial FTIR spectrometers, based on amplitude separation interferometers, have the drawback of being sensitive to vibrations, so that they require delay tracking with a He-Ne laser. In addition, they require careful alignment and are bulky by design, as they separate spatially the IR radiation. Our approach, based on a birefringent interferometer using the TWINS design, is very compact, requires only easy and fast alignment and is far less sensitive to vibrations.

Optics EXPRESS

In addition, it guarantees excellent delay accuracy and long-term stability. Calomel combines high birefringence (n_e-n_o≈0.55) with a broad transparency range (0.38-20 μm). Its present drawbacks are high manufacturing costs, due to processing difficulties, and the relatively low throughput, due to the large Fresnel losses. We measured an overall transmission of 19% at a delay where the two replicas do not interfere. Despite some efforts, an appropriate material that adheres to the surface of Calomel and could be used for an antireflection coating was not yet found. Calomel is also a very sensitive material that does not support large temperature changes that may occur in a coating chamber. One possibility of decreasing Fresnel losses is to reduce the number of interfaces by combining block A with the static wedge of block B in Fig. 1(a). This would also prevent any reflection from reaching the sample or detector. In the current scheme multiple reflections from the static block A could lead to interference, but we did not observe any significant effect on the data. If the coating problems are solved, we envisage that our compact FTIR can find several commercial applications in instruments with enhanced compactness, stability and portability.

Already in the present form, the special properties of TWINS are very favorable for more demanding FTIR methods. In step-scan FTIR, for example, the interferometer needs to stop repeatedly at a series of delays, where mirrors must be held stable to within ± 1.5 nm (equivalent to ± 0.8° of a He-Ne cycle) for sensitive biophysical measurements [33]. This value is very close to the phase stability of our TWINS, as revealed in Fig. 2. In high-end beam-splitting spectrometers such high stability usually requires operation of the interferometer under vacuum and removal of all sources of vibration (including sound) from the laboratory. In contrast, the data in Fig. 2 was recorded in a loud femtosecond laser laboratory, the He-Ne laser was located at 5 meters from the set-up, and the wedges were fixed on low-stability mounts. We are confident that we could easily improve stability by using better mechanical parts and by isolating better the setup from vibrations. In case, a feedback loop could also be easily implemented to reach even higher stabilities. We thus believe that calomel TWINS can become a viable alternative to complex and expensive step-scan technology. VCD is a further potential application for TWINS. In fact, polarization division interferometers with spatial beam separation have been used for VCD spectroscopy already a long time ago [34], and were recently developed for VCD experiments with femtosecond pulses [35, 36]. Calomel TWINS naturally produces two replicas of the input light with mutually perpendicular and high purity polarization, which is required for this form of chiral spectroscopy. It also has the long-term phase stability needed for detecting very small signals by averaging.

The advantages of phase stability, compactness and simplicity also apply to the 2DIR setup. With respect to our previous implementations of 2DES and 2DIR, we have further simplified the apparatus by using only two wedges. This was possible because of the small dispersion of calomel in the mid-infrared. However, Fresnel losses are currently very large and they reduce the intensity of the pump pulses by a factor of five. An interesting wavelength region to explore by 2DIR with calomel TWINS lies between 10 and 20 micrometers, where common IR-substrates like BaF_2 and CaF_2 are no longer transparent.

Funding

European Research Council: Advanced Grant STRATUS (ERC-2011-AdG No. 291198) and Proof of Concept Grant MISSION (ERC-2014-POC No. 665635). Marie Curie actions (FP7-PEOPLE-IEF-2012 No. 328110). Horizon 2020 (654148, Laserlab-Europe).

Acknowledgments

We would like to thank Olga Bozovic for providing the Rhenium sample used in the 2DIR measurements. We also thank Pascal Tournois, Hervé Jousselin and Nicolas Forget from Fastlite for fruitful discussions, and Cestmir Barta and Radek Hasal from BBT-Materials Processing, s.r.o. (Ltd.) for manufacturing the Calomel wedges and plates.